Journal of Magnetics 31(2), 187-194 (2026)
ISSN (Print) 1226-1750
ISSN (Online) 2233-6656
https://doi.org/10.4283/JMAG.2026.31.2.187

Magnetic Properties Measurement and Core Loss Modeling of Fe-Si Steel Sheet Using an Improved RSST

Yongjian Li[1]*, Baoliang Zhao[1], Shuaichao Yue[1], Yuan Liu[1], Yating Li[1,2], and Fei Zhao[3]

[1]State Key Laboratory of Intelligent Power Distribution Equipment and System, Hebei University of Technology, Tianjin 300401, China
[2]School of Engineering, Cardiff University, Cardiff CF24 3AA, United Kingdom
[3]Qingdao Yunlu Advanced Materials Technology Co., Ltd., Qingdao 266232, China

(Received 11 March 2026, Received in final form 26 May 2026, Accepted 28 May 2026)

Rotational magnetization has been widely observed in the T-joints of three-phase transformers and in motor stators. The resulting rotational losses are significantly higher than those measured under alternating magnetization conditions. To enable more accurate electromagnetic design and hotspot detection in electrical apparatus, an improved round rotational single sheet tester (RSST) with a large sensing area and large size samples is developed, providing a more representative characterization of the material's global magnetic anisotropy. In this paper, non-oriented (NO) silicon steel B25AV1300 and grain-oriented (GO) silicon steel B30P100 are measured under both alternating and rotating magnetic fields. Their magnetic field trajectories and loss characteristics under circular and elliptical excitations are analyzed and compared. Two core loss models are then proposed. The first model addresses one-dimensional alternating magnetization by predicting losses across flux densities and magnetization angles, whereas the second model characterizes two-dimensional rotational magnetization by predicting losses for flux densities over a defined ellipticity range. The accuracy of both models is validated experimentally.

Keywords : magnetic properties, round rotational single sheet tester, core loss modeling, silicon steel

1. Introduction

Silicon steel sheets are used extensively in energy-conversion devices, including transformers and rotating electrical machines, where they serve as the core magnetic material [1, 2]. Understanding their magnetization characteristics and loss behavior is therefore essential for developing reliable models for predicting magnetic performance and ensuring accurate electromagnetic and thermal design. Under practical operating conditions, the magnetization state of silicon steel is not restricted to purely one-dimensional alternating excitation. Alternating and rotating magnetizations coexist in various regions of electrical apparatus, particularly in the air-gap magnetic fields of alternating-current (AC) machines, transformer core T-joints, and leakage flux paths among three-phase windings. In these regions, the magnetic flux density vector continuously varies in both magnitude and direction, producing rotational magnetic field trajectories that may be circular or elliptical. Such multidirectional magnetization significantly increases the complexity of core-loss evaluation because the conventional alternating-loss assumption is no longer valid. Experimental investigations have shown that the core loss under rotational magnetization is substantially higher than that under conventional alternating magnetization, particularly in the linear region of the B–H curve, where rotational effects are often underestimated [3-5]. Consequently, loss evaluation based solely on alternating magnetic properties can lead to systematic underestimation of losses in practical devices. A thorough investigation of rotating magnetic properties is therefore essential for accurate material selection, reliable loss estimation, and optimal electromagnetic design of modern electrical systems.

The magnetic properties under rotating magnetization have been studied extensively. In [6], a rotating magnetic measurement system employing a U-shaped magnetic yoke was designed. In [7], a rotating magnetic measurement system with a C-shaped magnetic yoke and an asymmetric structure was developed. In [8] and [9], the

*Corresponding author: Tel: +86 13802065108
e-mail: liyongjian@hebut.edu.cn

authors developed a rotating magnetic measurement systems using a symmetric C-shaped magnetic yoke and ultra-thin silicon steel material. However, most existing rotational magnetic measurements employ cross-shaped samples, which have limitations such as small sample size and small sensing areas. As a result, the measurements are highly sensitive to local magnetic field non-uniformities and edge effects. Furthermore, the excitation conditions in many existing test systems are restricted to specific rotational trajectories or limited magnetization states, reducing their ability to characterize the overall magnetic anisotropy of the material. Consequently, the resulting loss data are often difficult to incorporate directly into practical core-loss prediction models for electrical devices. Therefore, improved rotating magnetic characterization methods that can provide representative loss data under a wide range of excitation conditions are urgently needed; these methods will enable more accurate loss evaluation and electromagnetic design. In [10] and [11], the authors proposed complex-valued rotational magnetic property model and an analytical core-loss model based on vector magnetic circuit theory, respectively. Although these approaches provide valuable insights, they involve high computational costs and are not well suited to rapid engineering calculations. In [12], a rotational loss model considering ellipticity was proposed; however, its prediction accuracy remains limited.

In this paper, the design of the measurement system, experimental investigations, and development of the proposed loss prediction models are presented. A one-dimensional loss model is developed by considering both magnetic flux density and magnetic anisotropy, achieving prediction errors generally below 3%. By optimizing the existing model for flux density and varying ellipticity, the two-dimensional model improves the prediction accuracy from 2.11% to 0.73%.

2. Rotational Measurement System

In this study, an improved RSST measurement system incorporating circular excitation, large-size circular samples, an enlarged sensing area, and an amorphous alloy laminated sheet yoke are employed to measure the alternating and rotational magnetic properties of silicon steels. Circular excitation provides a larger uniform magnetic field region; large-size circular samples facilitate alternating-field measurements at different angles, reduce material consumption, and enable spatial averaging of magnetic properties, resulting in a more representative characterization of overall material behavior. The enlarged sensing area improves sensor sensitivity and reduces measurement errors. In addition, the amorphous alloy yoke exhibits excellent high-frequency performance, enabling the measurement system to operate at a higher upper frequency limit [13-15].

Fig. 1. shows a schematic diagram of the rotating measurement system. In this system, a circular magnetic yoke is used. Dual-channel excitation signals with independently controllable amplitudes and phase angles are generated using LabVIEW. Using the effective feedback control strategy developed in this work, a highly uniform magnetic flux density distribution $\boldsymbol{B}$ can be achieved within the measurement region. The excitation signals generated by LabVIEW are transmitted through the analog output channels of a data acquisition card (DAQ, NI PXIe-6368) and subsequently amplified by a power amplifier. To improve excitation capability, particularly at high frequencies, the excitation winding is connected in series with an adjustable matching capacitor. This arrangement compensates for the phase angle between the excitation voltage and current, thereby achieving a larger excitation current. Six signals are obtained from the ***B-H*** composite magnetic sensor structure, namely U_{BX}, U_{BY}, U_{HX1}, U_{HX2}, U_{HY1} and U_{HY2}, corresponding to the magnetic flux density $\boldsymbol{B}$ and magnetic field strength $\boldsymbol{H}$ components in the x and y directions. The spacing between the ***B***-probes b is 40 mm, and the size of the **H**-coils is 35 × 17 mm. The compo-0 nents of the magnetic flux density $\boldsymbol{B}$ along each axis are calculated using Eq. (1) as follows:

$$B_i = \frac{2}{bt}\int U_{Bi}dt, i = x, y \tag{1}$$

where, b is the distance between each pair of needles, t is the sample thickness, and U_{Bi} is the instantaneous induced voltage measured across each pair of needles. The $\boldsymbol{H}$

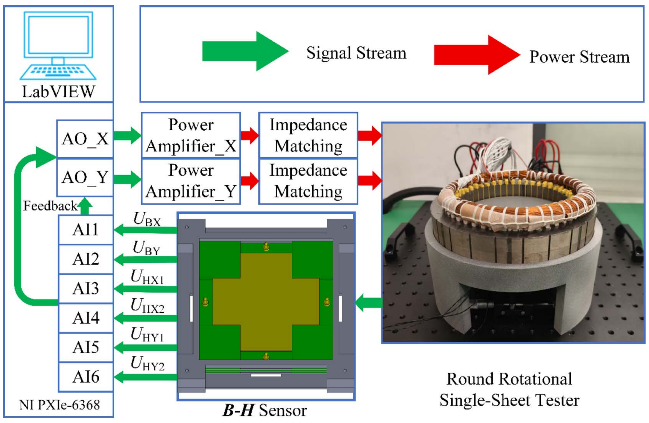

Fig. 1. (Color online) Rotational measurement system using circular magnetic yoke.

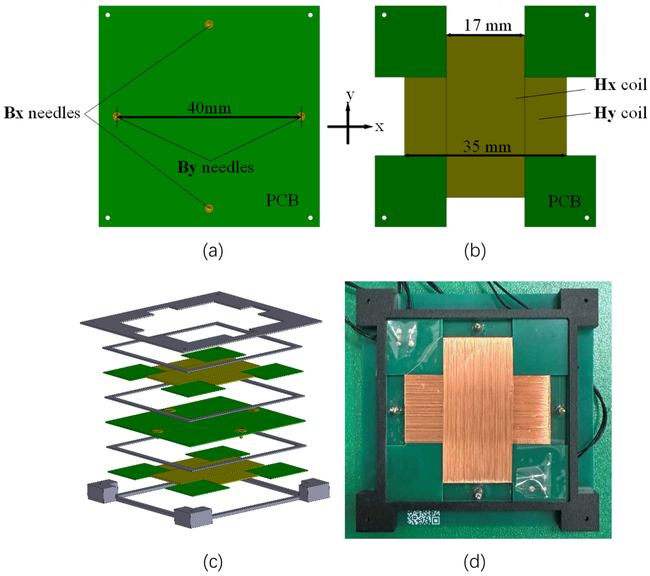

Fig. 2. (Color online) Sensor display (a) PCB board with B probes; (b) PCB board with H coils; (c) sensor structure; and (d) photograph of the sensor.

components are determined using Eq. (2) as follows:

$$H_{ij} = \frac{1}{\mu_0 K_{\mathrm{H}i}} \int U_{\mathrm{H}_{ij}} dt, i = x, y; j = 1, 2 \quad (2)$$

where, μ_0 is the magnetic constant, $K_{\mathrm{H}i}$ is the coefficient of ***H***-coil and $U_{\mathrm{H}ij}$ is the instantaneous induced voltage across each coil. The sensor configuration is illustrated in Fig. 2. The sensor coil terminals are twisted to reduce the influence of stray fields. To more accurately characterize the magnetic field strength on the sample surface, we adopted a double-layer ***H***-coil configuration in the sensor design. The magnetic field strength ***H*** is calculated using Eq. (3) as follows:

$$H_i = \frac{h_2 H_{i1} - h_1 H_{i2}}{h_2 - h_1}, i = x, y \quad (3)$$

where h_1 and h_2 are the distances from the two ***H***-coils to the sample respectively, and H_{i1} and H_{i2} represent the corresponding magnetic field strengths. A differential amplifier is used to amplify the output signal of the sensor before sending it to the analog input ports of the DAQ card. The two-dimensional rotational core loss is calculated based on the magnetic flux density ***B*** within the sample and the magnetic field strength ***H*** on the sample surface. Based on Poynting's theorem [16], the total core loss (W/kg) is expressed by Eq. (4)

$$P = \frac{f}{\rho} \int_0^T (H_x \frac{dB_x}{dt} + H_y \frac{dB_y}{dt}) dt \quad (4)$$

where ρ is the mass density of the sample (kg/m^3), f is the magnetization frequency (Hz), T is the time period (s), B_x and B_y are the orthogonal components of B and H_x and H_y are the orthogonal components of H.

3. Measurement Results and Discussion

Using the rotating magnetic measurement system shown in Fig. 1, the following experiments are carried out: alternating magnetic property tests and rotating magnetic property tests on NO steel B25AV1300 and GO steel B30P100. The rotational magnetization tests are performed under two excitation modes: circular and elliptical excitation conditions. The NO and GO samples are circular, with diameters of 150 mm and thicknesses of 0.25 mm and 0.30 mm, respectively.

3.1. Alternating magnetic properties analysis

The results of measurements obtained under one-dimensional alternating magnetization are shown in Fig. 3. The hysteresis loops and core loss curves of the NO steel along the RD and TD are shown in Fig. 3(a), and the corresponding results for the GO steel are shown in Fig. 3(b); both measurements are conducted at 400 Hz. For the NO steel, although the hysteresis loops along the rolling direction (RD) and transverse direction (TD) directions are similar at low magnetic flux densities, noticeable differences arise at higher flux densities, with the permeability along RD being slightly higher than that along TD. For the GO steel, the strong Goss texture produces a substantially higher permeability along the RD than along the TD, resulting in pronounced differences between the hysteresis loops in the two directions.

At a flux density ***B*** of 1.5 T, the core loss of the NO steel measured along TD is 35.07 W/kg, which is 34.7% higher than that along RD (26.04 W/kg). For the GO steel, at a flux density ***B*** of 1.4 T, the loss in the TD reaches 47.92 W/kg, which is several times greater than RD loss of 19.95 W/kg. These findings are consistent with previously reported results [17]. In modeling practice, NO steel is usually assumed to be isotropic; however, its actual magnetic anisotropy increases the discrepancy between simulation results and experimental measurements.

3.2. Rotational magnetic properties analysis

Fig. 4 shows the averaged ***B*** and ***H*** waveforms measured at 400 Hz under both clockwise (CW) and anticlockwise (ACW) rotation, in order to eliminate errors arising from sensor misalignment. In the 2-D rotational magnetization measurements, the *x*-axis of the measurement system is aligned with the TD of the sample, while

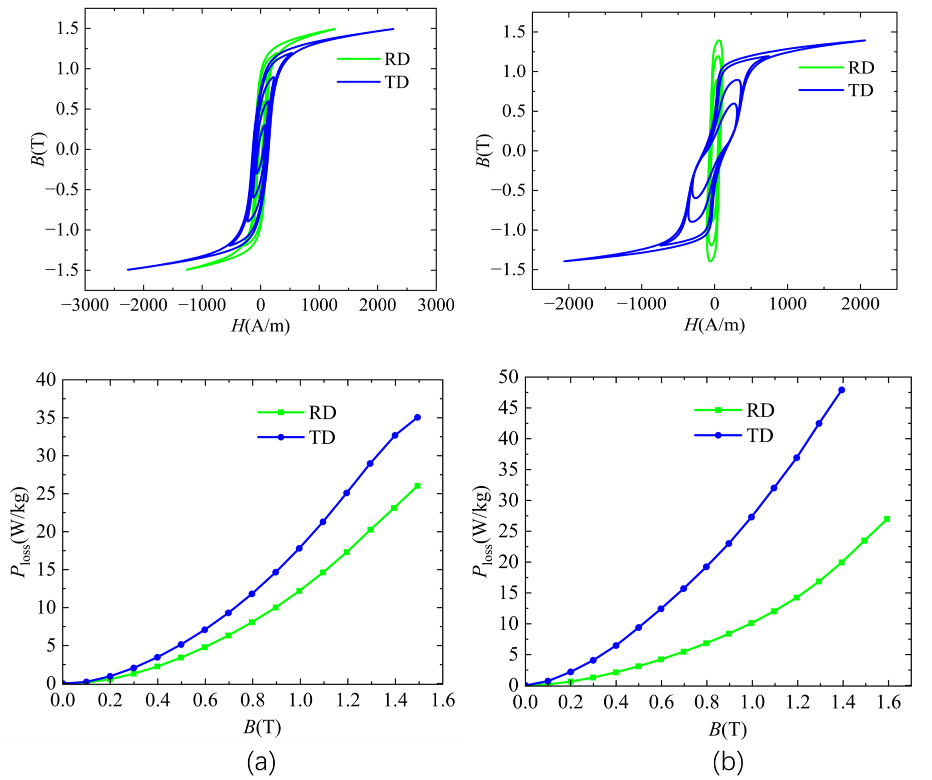

Fig. 3. (Color online) Measurement results along RD and TD at 400 Hz: (a) NO steel (left) and (b) GO steel (right).

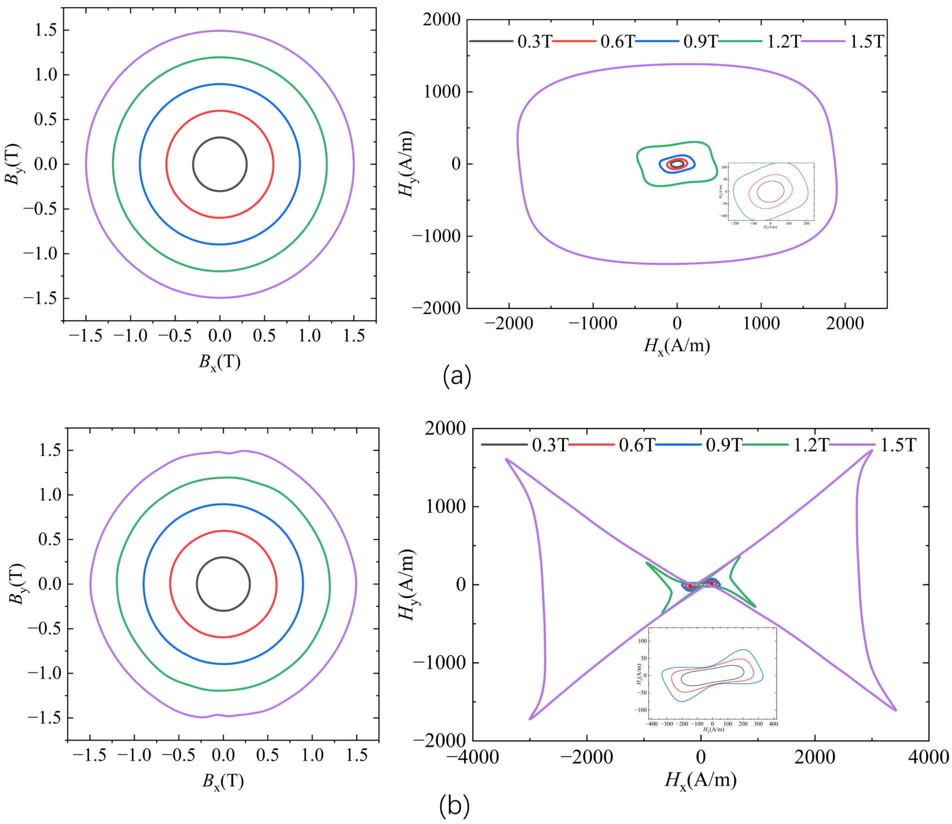

Fig. 4. (Color online) Loci of vector B (left) and corresponding H (right) in NO and GO steels under circular rotational magnetizations at 400 Hz: (a) NO steel and (b) GO steel.

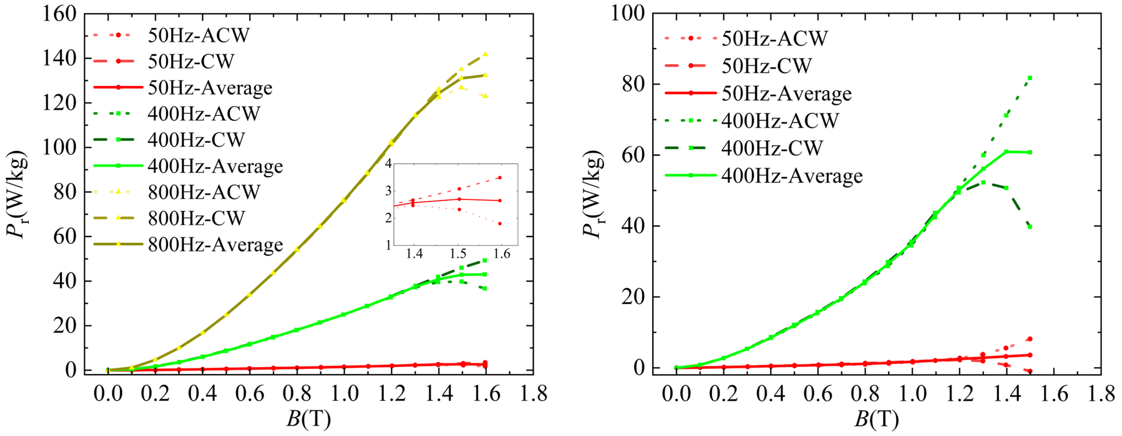

(a) (b)

Fig. 5. (Color online) Measured ACW, CW and average core loss: (a) NO steel and (b) GO steel.

the *y*-axis is aligned with RD. The system maintains nearly circular trajectories for the magnetic flux density ***B***. In contrast, the *H* trajectories vary significantly with the magnetic flux density level. For NO steel B25AV1300, the ***H*** locus gradually evolves from an elliptical shape to a saddle shape as ***B*** increases. In contrast, for the GO steel B30P100, the ***H*** trajectory transitions more rapidly into a saddle- shaped pattern with increasing ***B***. These behaviors originate from the anisotropy of the materials.

The rotational core-loss characteristics of the two materials under different frequencies and orientations are shown in Fig. 5. The curves can be interpreted in two regions. In the low-flux-density region, the reversible motion of domain walls is sufficient to support magneti-

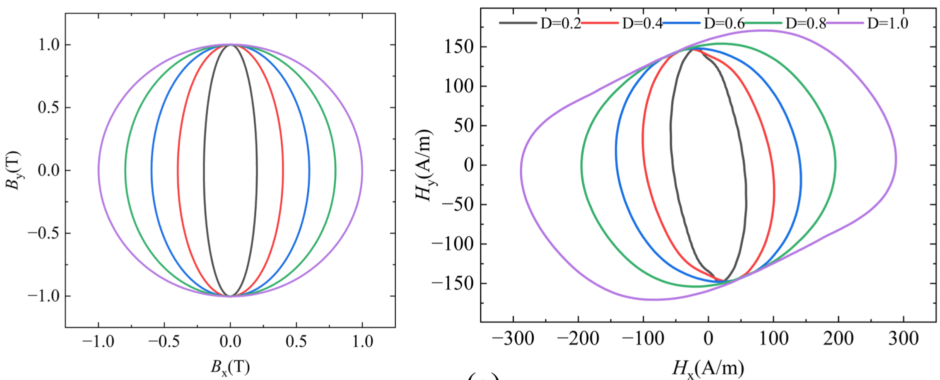

(a)

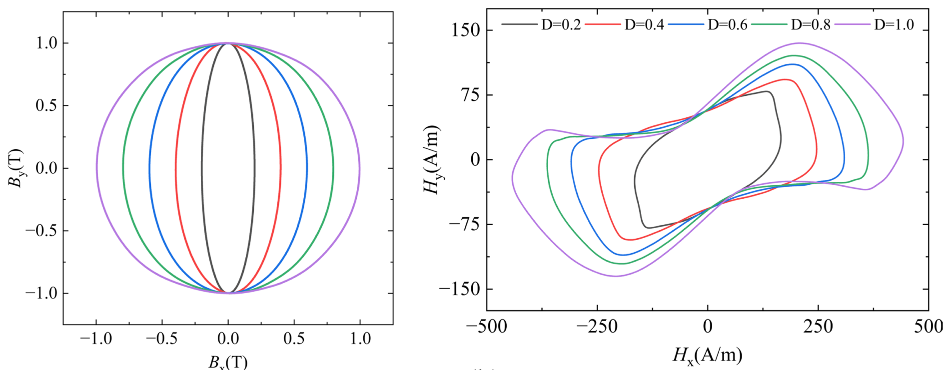

(b)

Fig. 6. (Color online) Loci of B (left) and corresponding H (right) under elliptical magnetizations at 800 Hz: (a) NO steel and (b) GO steel.

zation in all directions, and the rotational loss exhibits behavior similar to that observed under alternating magnetization. In the high-flux-density region, domain magnetization begins to rotate in order to further increase the magnetization. As the number of active domains decreases, the corresponding hysteresis loss and anomalous loss gradually reduce, resulting in a decrease in total loss [18-20]. Comparison of the core loss curves, as shown in Fig. 5. and Fig. 3, indicates that the rotational core loss approximates the superposition of alternating core losses along two orthogonal directions in the low flux density region, whereas it becomes significantly lower than their sum in the high flux density region.

In addition to circular rotational magnetization, elliptical magnetization with different axis ratios was applied to both materials, as shown in Fig. 6. To approximate the practical operating conditions of silicon steel sheets, the flux density along RD is maintained at 1.0 T, while the flux density along the TD is stepped from 0.2 T to 1.0 T, producing a series of curves with ellipticities ranging from 0.2 to 1.0.

4. Core Loss Modeling

4.1. Alternating core loss modeling

An alternating loss model for NO steel is established based on the conventional Bertotti loss separation model combined with an analytical approach. Because the influence of frequency on core loss is well established, in the proposed model, only the effects of magnetization angle and flux density on the loss are considered. The alternating loss can be expressed as (5):

$$P_{\mathrm{alt}}(B,\theta)=P_{\mathrm{RD}}(B)+[P_{\mathrm{TD}}(B)-P_{\mathrm{RD}}(B)]\bullet g(\theta) \quad (5)$$

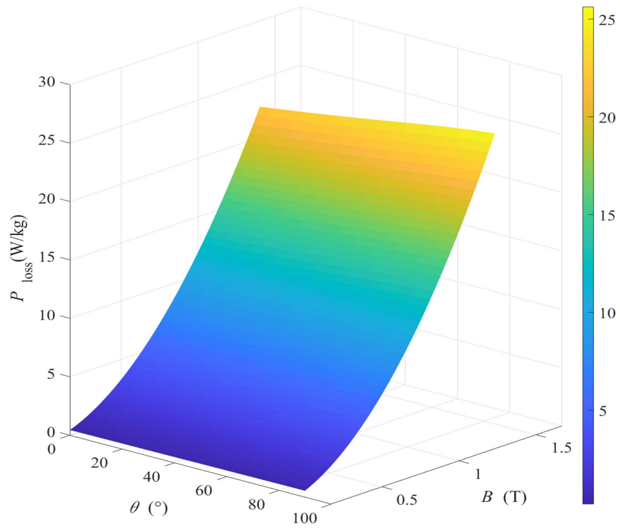

Fig. 7. (Color online) Predicted alternating core loss results.

where θ denotes the angle between the excitation direction and RD, ranging from 0° to 90°. $P_{\mathrm{RD}}(B)$ and $P_{\mathrm{TD}}(B)$ represent the losses corresponding to RD and TD, respectively, at a given flux density B, and they are obtained using the conventional Bertotti loss model. The function $g(\theta)$ is fitted using a trigonometric polynomial.

A three-dimensional visualization of the loss prediction results based on the model in (5) is shown in Fig. 7. The core loss increases approximately exponentially with increasing B and increases moderately with increasing θ. The influence of θ becomes more pronounced in the high-flux-density region. For applications that require high accuracy, anisotropic modeling or 2-D magnetic property modeling of the material is therefore necessary.

The experimental validation of the proposed model is shown in Fig. 8. The experimental results are obtained by

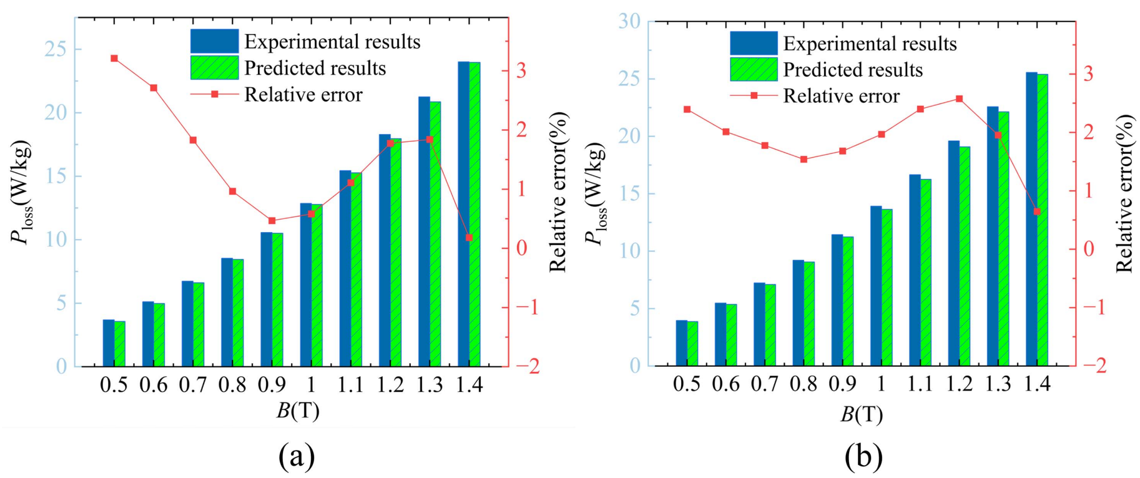

Fig. 8. (Color online) Experimental verification of the model at (a) 40° and (b) 80°.

averaging multiple measurements to reduce the influence of random variations. The proposed model demonstrates high prediction accuracy, with the relative error generally not exceeding 3%.

4.2. Elliptical core loss modeling

An elliptical rotational loss model is developed by optimizing the analytical method proposed in [12]. In this model, the ellipticity is defined by Equation (6):

$$D = \frac{B_x}{B_y} \tag{6}$$

where B_x denotes the magnetic flux density along the x-axis, corresponding to TD, and B_y denotes the magnetic flux density along the y-axis, corresponding to RD. The ellipticity D ranges from 0 to 1. When D = 0, the excitation corresponds to 1-D magnetization along the RD, whereas when D = 1, the excitation represents circular magnetization. The equivalent flux density B_{eq} is defined by Eq. (7).

$$B_{eq} = \sqrt{B_x^{\,2} + B_y^{\,2}} \tag{7}$$

The elliptical rotational loss can then be expressed by Eq. (8)

$$P_t = DP_r + (1-D)^2 P_{alt} \tag{8}$$

where P_r denotes the circular rotational core loss at the corresponding flux density level and P_{alt} represents the weighted average of the alternating losses along the RD and TD at the equivalent flux density B_{eq}. P_{alt} can be calculated using Equation (9):

$$P_{alt} = \frac{1}{1+D} P_{RD} + \frac{D}{1+D} P_{TD} \tag{9}$$

The correctness and accuracy of the proposed model is verified by defining the error using Equation (10) as follows:

$$\text{Error} = \frac{\sqrt{\frac{1}{N-1}\sum_{i=1}^{N}(P_{test} - P_{cal})^2}}{\max(P_{test})} \tag{10}$$

where N denotes the number of data points used for validation, P_{test} represents the test data obtained by averaging multiple measurements, and P_{cal} denotes the model-predicted data. While the model reported in [10] yields an error of 2.11%, the optimized model reduces this error to 0.73%.

5. Conclusion

In this paper, a customized RSST with an amorphous-material yoke is employed to measure the 1-D magnetic properties of NO and GO steels along different angles and 2-D magnetic properties under varying ellipticities. It is found that even NO steel exhibits a certain degree of magnetic anisotropy, whereas the GO steel demonstrates pronounced anisotropy. Owing to the influence of magnetic domains, the core loss under circular magnetization initially increases but then decreases. Based on the measurements, a 1-D loss model accounting for anisotropy and an elliptical loss model considering the axial ratio are proposed. Both models show good agreement with the experimental results. The measured data and proposed models can be used for core loss modeling and design optimization in rotating machines and transformers.

Acknowledgment

This work was supported by the National Natural Science Foundation of China under Grant Nos. 52130710 and 52407005.

References

[1] H. Pfutzner, E. Mulasalihovic and H. Yamaguchi, IEEE Trans. Magn. **47**, 4523 (2011).
[2] Y. Guo, J. G. Zhu, J. Zhong, H. Lu and J. X. Jin, IEEE Trans. Magn. **44**, 279 (2008).
[3] T. Sasaki, M. Imamura, S. Takada and Y. Suzuki, IEEE Trans. Magn. **21**, 1918 (1985).
[4] C. Ragusa, C. Appino, and F. Fiorillo, J. Magn. Magn. Mater. **316**, 454 (2007).
[5] E. Dlala, A. Belahcen, and A. Arkkio, IEEE Trans. Magn, **46**, 3101 (2010).
[6] S. Huang, C. Stefano Ragusa, W. Xu, L. Solimene, and S. Wang, IEEE Trans. Ins. Meas. **74**, 6004511 (2025).
[7] Y. Dou, Y. Li, Z. Lin, S. Yue, and J. Zhu, IEEE Trans. Ins. Meas, **71**, 6000210 (2022).
[8] J. Gao, S. Yue, Y. Dou, J. Zhou, J. Yin, and Y. Li, IEEE Trans. Ins. Meas, **74**, 6000408 (2025).
[9] D. Zhang, K. Shi, Z. Ren, M. Jia, C.-S. Koh, and Y. Zhang, IEEE Trans. Ind. Electron. **69**, 980 (2022).
[10] Y. Zhang, Y. Liu, Y. Li, D. Xie, and B. Bai. IEEE Trans. Magn. **50**, 7009704 (2014).
[11] C. Li, M. Cheng, W. Qin, Z. Wang, X. Ma, and W. Wang, IEEE Open J. Power Electron. **5**, 1659 (2024).
[12] P. C. Sarker, Y. Guo, H. Y. Lu, and J. G. Zhu, IEEE Trans. Magn. **57**, 8402008 (2021).
[13] J. C. Akiror, J. Wanjiku, P. Pillay, J. Cave, and A. Merkhouf, IEEE Trans. Ind. Appl. **54**, 4355 (2018).

[14] B. S. Abdel-Mageed, M. Ibrahim, J. Bhalala, and P. Pillay, IEEE Trans. Ind. Appl. **59**, 3278 (2023).
[15] J. Wanjiku and P. Pillay, IEEE Trans. Ind. Appl. **52**, 3022 (2016).
[16] K. Atallah and D. Howe, IEEE Trans. Magn. **29**, 3547 (1993).
[17] C. Appino, E. Ferrara, and F. Fiorillo, Int. J. Appl. Electromag. Mech. **48**, 123 (2015).
[18] S. Yue, Y. Li, Q. Yang, K. Zhang, and C. Zhang, IEEE Trans. Magn. **55**, 6100705 (2019).
[19] J. Li, Q. Yang, and Y. Li, IEEE Trans. Magn. **54**, 4300205 (2018).
[20] J. Ding, L. Li, and X. W. Zhang, Adv. Technol. Electr. Eng. Energy **41**, 72 (2022) (in Chinese).